A Mechanically-Robust and Spectrally-Selective Convection Shield for Daytime Sub-Ambient Radiative Cooling

Journal:	*ACS Applied Materials & Interfaces*
Manuscript ID	am-2020-21204y.R2
Manuscript Type:	Article
Date Submitted by the Author:	n/a
Complete List of Authors:	Zhang, Ji; Tianjin University Zhou, Zhihua; Tianjin University Tang, Huajie; Tianjin University Xing, Jincheng; Tianjin University Quan, Jiayou; Donghua University Liu, Junwei; Tianjin University Yu, Junrong; Donghua University Hu, Mingke; University of Nottingham,

A Mechanically-Robust and Spectrally-Selective Convection Shield for Daytime Sub-Ambient Radiative Cooling

Ji Zhang[a], Zhihua Zhou[a], Huajie Tang[a], Jincheng Xing[a], Jiayou Quan[b], Junwei Liu[a], Junrong Yu[b], Mingke Hu[c*]*

a. *Tianjin Key Laboratory of Indoor Air Environmental Quality Control, College of Environmental Science and Engineering, Tianjin University, Tianjin 300350, China.*

b. *State Key Laboratory for Modification of Chemical Fibers and Polymer Materials, College of Materials Science and Engineering, Donghua University, Shanghai 201620, China.*

c. *Department of Architecture and Built Environment, University of Nottingham, University Park, Nottingham NG7 2RD, UK.*

Corresponding Author: Mingke Hu

Tel.: +44-0115-84-67872

E-mail address: Mingke.Hu@nottingham.ac.uk

Co-Corresponding Author: Junrong Yu

Tel.: +86-216-7792945

E-mail address: yjr@dhu.edu.cn

A Mechanically-Robust and Spectrally-Selective Convection Shield for Daytime Sub-Ambient Radiative Cooling

ABSTRACT

As a passive cooling strategy, radiative cooling becomes an appealing approach to dissipate heat from terrestrial emitters to outer space. However, current achieved cooling performance still underperforms due to considerable solar radiation absorbed by the emitter and non-radiative heat transferred from the surroundings. Here, we proposed a mechanically-robust and spectrally-selective convection shield composed of nanoporous composite fabric (NCF) to achieve daytime sub-ambient radiative cooling. By selectively reflecting ~95% solar radiation, transmitting ~84% thermal radiation, and suppressing the non-radiation heat transferred from warmer surroundings, the NCF-based radiative cooler demonstrated an average daytime temperature reduction of ~4.9 °C below the ambient, resulting in an average net radiative cooling power of ~48 W/m^2 over the 24-hour measurement. In addition, we also modeled the potential cooling capacity of the NCF-based radiative cooler and demonstrated that it can cover cooling demand of energy-efficient residential buildings in most regions of China. Excellent spectral selectivity, mechanical strength, and weatherability of the NCF cover enable a much broader selection for the emitters, which is promising in real-world deployment of direct daytime sub-ambient radiative cooling.

KEYWORDS

Radiative cooling, convection shield, composite film, mechanically-robust, spectrally-selective

TABLE OF CONTENTS GRAPHIC

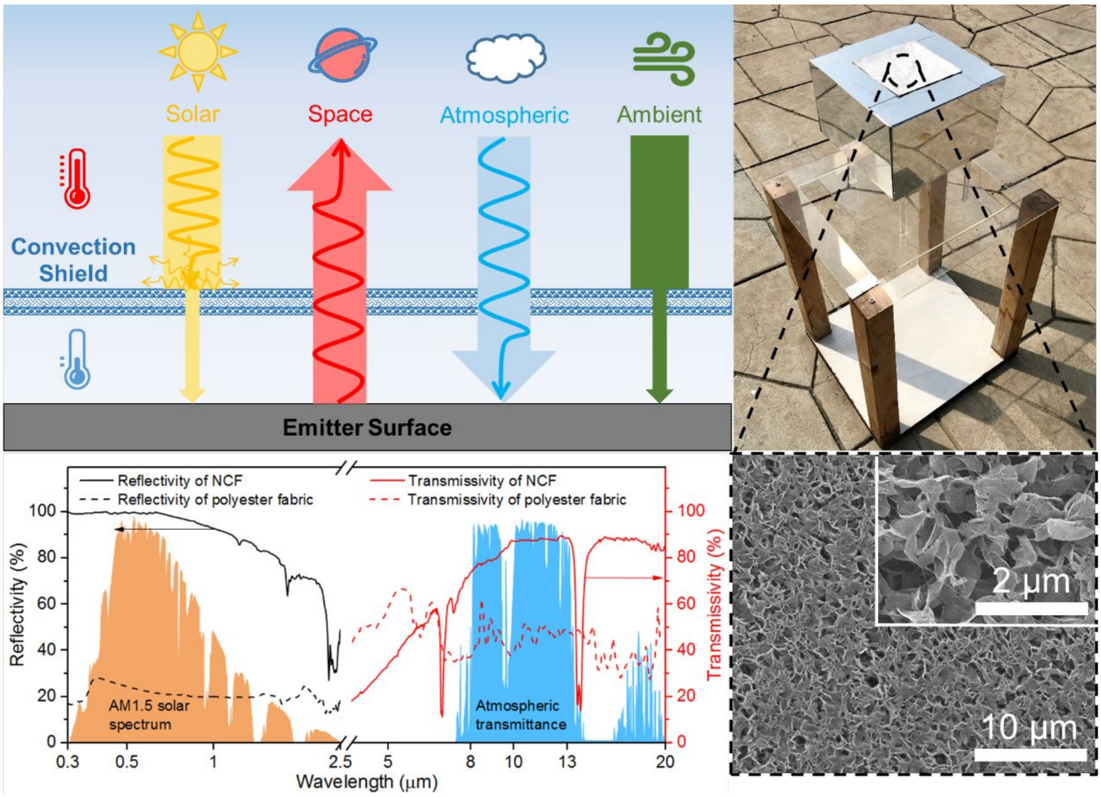

INTRODUCTION

Radiative cooling is a passive cooling strategy to emit thermal infrared (IR) radiation into the deep universe through the atmospheric transparent window (ATW) of 8-13 μm,[1] without consuming extra energy or producing environmental pollution.[2] Remarkable developments have been made in the last decade, particularly with the breakthrough of daytime radiative cooling. Theoretically, an ultra-large temperature reduction of 60 °C below ambient, and a net cooling power of more than 100 W/m^2 is achievable at ambient temperature.[3] However, experimentally demonstrated temperature reduction still underperforms.[4] The principal reason behind this phenomenon is the considerable absorption of solar radiation and the undesirable non-radiative heat transferred from warmer surroundings.

Above all, intense solar irradiance (~1000W/m^2) is a tough handicap for daytime radiative cooling,[5] due to the lower energy flux of outward thermal radiation (100 – 150 W/m^2 depending on surface temperature).[6] It has been proved that even a 1% increase in solar absorption of the emitter will decrease its cooling power by ~10%.[7] Therefore, minimizing solar absorption is significant for daytime radiative cooling applications. Recently, various engineered cooling materials have been proposed to reflect solar radiation. These strategies can be divided into two main categories as self-reflecting emitters and reflective covers.

Self-reflecting emitters (see Figure 1A) barely absorb solar radiation due to high solar reflectivity, but they generally require heat conduction between the emitter and the object to be cooled.[8] The solar reflectivity of the emitters can be obtained by either combining the emitter with a back metal reflector (silver or aluminum)[9,10] or employing Mie scattering to reduce solar absorption, including particle-based coatings[11,12] and porous materials.[13,14] Despite abundant sub-ambient radiative cooling experiments that have been demonstrated,[15] the deposition process and oxidation problem of reflective layers limit the practical applications. Besides, some white particles are effective ultraviolet (UV) absorbers,[16] which degrades the solar reflection.[17]

In contrast, reflective covers (see Figure 1B) reflect solar radiation and are transparent for IR radiation at the same time, allowing the object beneath to emit heat to outer space.[18] Thus, it can be referred to as a direct radiative cooling approach, spatially decoupling the demand of solar reflection from the thermal emitter. Reflective covers are generally made of low IR-absorptivity materials with high porosity,[19] which have been used as personal thermal management textiles.[20] Porous structures in reported materials were either prepared by electrospinning[21] or extraction of a sacrificial phase.[22] Kim et al. prepared electrospun polyacrylonitrile nanofibers (NanoPAN) with a solar reflectivity of 95% and an IR transmissivity of 70%. However, achieving precise control over the morphology of nanofibers remains challenging.[23] Torgerson et al. fabricated the polymer filter (STATIC) by extracting sacrificial particles of ZnO in the composite of polyethylene resin, which may bring inconvenience and incomplete treatment.[24] Similarly, a 6-mm-thick polyethylene aerogel (PEA) with a solar reflectivity of 92.2% and an atmospheric window transmissivity of 79.9% was developed via thermally induced phase separation (TIPS) of paraffin oil.[25] Although the above materials have achieved daytime sub-ambient radiative cooling, the mechanical strength needs to be further improved to meet the demands for practical applications.

In addition to solar absorption, non-radiative heat transferred between the surroundings and the emitter surface is another important factor that limiting the cooling performance in sub-ambient scenarios. Studies have shown that the non-radiation heat transfer coefficient (h_c) can reach up to 40 W/m^2·K when wind speed reaches 12 m/s,[26] indicating that it is difficult to realize sub-ambient temperature reduction if the non-radiation heat transferred cannot be effectively suppressed.[27] To combat this, convection shields that isolate emitters from the surroundings are required for sub-ambient radiative cooling.[28] To date, few materials have been proposed as desirable convection shields. For instance, ZnSe,[3] ZnS,[29] or CdS[30] cannot be used under direct sunlight during the daytime. Thin polyethylene (PE) films[31,32] lack durability and mechanical strength for outdoor applications. The cooling capacity of special-shaped configurations of PE, e.g. multilayer films,[33] corrugated structures,[34] and meshes[35] are undesired.

In this context, we proposed a mechanically-robust and spectrally-selective convection shield for daytime sub-ambient radiative cooling. The convection shield is composed of nanoporous composite fabric (NCF) using affordable materials via a scalable fabricating process. The NCF can not only suppress non-radiative heat transferred from warmer surroundings but also reduce absorbed solar radiation of the emitter surface, while maintaining high IR transparency to thermal radiation from the emitter simultaneously.

We first obtained the NCF endowed with a solar reflectivity of ~95% and an IR transmissivity of ~84% by optimizing the pore size using Mie theory. During outdoor cooling experiments for a NCF-based radiative cooler, we reported an average daytime sub-ambient temperature reduction of ~4.9 °C, and an average net radiative cooling power of ~48 W/m^2 over 24-hour period. We then demonstrated the durability performance of the NCF with desired mechanical strength, hydrophilicity, thermostability, and UV-resistance. Further simulation suggested that a temperature reduction as high as ~10 °C, and a considerable net radiative cooling power up to ~100 W/m^2 can be reached by equipping the NCF atop solar-reflecting emitters. Additionally, modeling results indicated that the NCF-based radiative cooler can cover cooling demand of energy-efficient residential buildings in most regions of China. This convection shield can be easily applied and removed on various substrates repeatedly, not only improving the cooling performance but also protecting the beneath objects from harsh weather. More compelling, the NCF mitigates the demanding spectral selectivity of the emitter, enabling more emitter materials with unfavorable solar reflectivity but good thermal emissivity to achieve direct sub-ambient daytime radiative cooling.

RESULTS AND DISCUSSION

Radiative Properties of the NCF. For daytime radiative cooling, the spectrally-selective convection shield should be designed as a solar-reflecting and IR-transparent shield. Thus, the PE is selected as the raw material for its intrinsically low IR absorptivity.[36] The optical properties of the PE (refractive index and extinction coefficient)[37] are represented in Figure S1. The absorptivity and transmissivity of a 100-μm-thick PE were modeled by the generalized transfer matrix method[38] as shown in Figure S2. The results show the existence of small absorption peaks around 3.5, 7, and 14 μm, corresponding to the stretching vibration of C−H and C−C bonds.[36] Despite that, the absorptivity is very low in the whole waveband, resulting in high transmissivity in the IR spectra.

Meanwhile, Mie scattering takes place in situations where the object size is comparable to the wavelength of the incident light.[39] Therefore, it is practicable to exploit scattering by size-controlled air pores to maximize solar reflectivity while maintaining high IR transmissivity.[40] By solving Maxwell's equations, the calculated scattering efficiency factor Q_{sca} is shown in Note S1. The Q_{sca} for air pores of specified radius are compared in Figure S3. Results show that the pore size is a critical parameter for scattering efficiency. With increasing the pore size, the scattering efficiency improves and tends to be stable with larger radiuses. However, the pore with a radius less than 0.2 μm scarcely interferes with IR radiation, guaranteeing the high transmissivity of PE. To obtain spectral selectivity with high solar reflectivity and high IR transmissivity, the Q_{sca} should be high enough in the solar spectrum and as low as possible in the ATW. To quantitatively optimize the pore size, we determined a comparative factor (η) as the ratio of the weighted average scattering efficiency in the solar spectrum to that in the ATW (see Note S2). As shown in Figure S4, the Q_{sca} in the solar spectrum plateaus when pore radius exceeds 0.5 μm, while that in the ATW keeps on upgrading. η drops sharply as the radius increases, which is acceptable with a value over hundreds,[24] meaning a striking contrast between the scattering efficiencies in the solar spectrum and the ATW. Accordingly, pores of radius between 0.2 and 0.5 μm are structurally designed in the NCF. The combination of intrinsic mid-IR transparent material and nanopores changes spectral response of the NCF to electromagnetic waves, thereby achieving selectively spectral control.

We then fabricated the NCF with paraffin oil as the diluent of ultrahigh molecular weight polyethylene (UHMWPE) via TIPS method[41] (see Figure 1E). Polyester woven fabrics were used as the composite medium to provide mechanical strength. A photograph of the fabricated NCF sample with a thickness of ~200 μm is shown in Figure 1C. The resultant NCF is flexible and has a balanced white color, which can effectively scatter incident light in a hemispherical solid angle, avoiding discomfort glare caused by strong specular reflection.[42] The pre- and post-treatment of the polyester fabric are compared with the optical microscopy images shown in Figure 1D. It can be observed that there are many large irregular holes between adjacent warp and weft yarns in the polyester fabric. After compositing, the polyester mesh is wrapped with the UHMWPE phase, without being destroyed under hot-compressing temperature.

Moreover, Figure 1F shows the typical internal porous structures of the surface and cross-section view of the NCF. The pore size distribution shown in Figure 1F-(i) indicates that the average diameter of the pores is about 0.825±0.418 μm. The existent of inter-connected nanopores can be clearly observed in the surface (see Figure 1F-(ii)) and cross-section view (see Figure 1F-(iii) and (iv)) SEM images. Comparatively, the pores in the cross-section view are denser and more flat than those in the surface view due to the preparation process of hot-compress. The polyester fabric is adequately wrapped in the surrounding UHMWPE phase, as shown in Figure 1F-(iii). The nanoporous structure eventually yields a high porosity of 84%, and a low bulk density of 0.21 g/cm^3, enabling the NCF to be more flexible for practical applications.

Thanks to the nanostructure and natural characteristics of the PE, the NCF exhibits a near-ideal spectral selectivity: strong solar reflectivity and high IR transmissivity (see Figure 1G). The weighted average solar reflectivity of the NCF is ~95% due to strongly scattering at short wavelengths (0.3 to 2.5 μm), while that of polyester fabric is only ~22%. Besides, the IR transmissivity of the NCF reaches ~84%, which is comparable to that of most available nanoporous materials,[43] while that of polyester fabric is only ~44.6%. The increased IR transmissivity of the NCF is attributed to two main reasons. First, the nanoporous UHMWPE around the polyester fibers decreases the reflected IR waves and helps to increase IR transmissivity.[44] Second, the internal structure of materials is crucial to transmissivity.[4546] Many UHMWPE phase nanopores are formed in the gaps of fabric after compositing, which diminishes the distance between the adjacent fibers in the polyester mesh and thus help to increase IR transmissivity. These optical properties are necessary for spectrally-selective convection shields to reflect solar radiation but transmit IR radiation. Cooling capacity of the NCF-based radiative cooler with different solar reflectivity and IR transmissivity is illustrated in Figure S5.

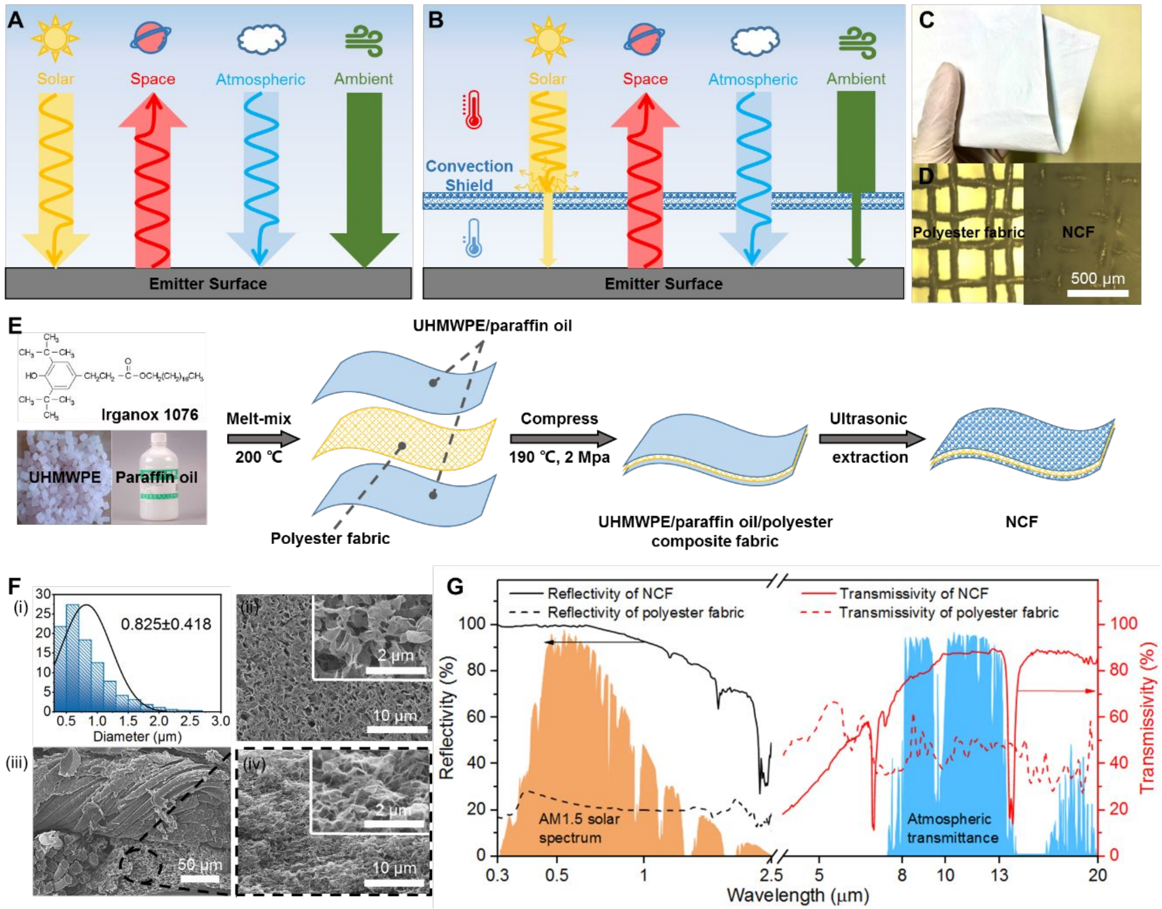

Figure 1. Optical property and morphology of the NCF. Schematic of (A) traditional radiative module and (B) spectrally coupled radiative module with a convection shield. (C) Photograph of an NCF sample. (D) Optical microscopy images of the polyester fabric (left) and the NCF (right). (E) Schematic outlining for fabricating the NCF. (F) Microstructure of the NCF. (i) Pore size distribution, SEM images of (ii) the surface view, (iii) cross-section view, and (iv) enlarged cross-section view. (G) Solar reflectivity and IR transmissivity of the NCF. Normalized AM1.5 solar spectrum[47] and atmospheric transmittance are shown for reference.

Cooling Performance Measurements. We measured the radiative cooling performance using the NCF with a black emitter during both day and night over a continuous 24-hour period in Tianjin, China (39.13°N, 117.2°E; 3.5-m altitude). We firstly compared the stagnation temperatures of the bare cooling device (see Figure 2A) and the NCF-based radiative cooling device (see Figure 2B). The two devices were placed side by side and supported by 1000-mm-height wooden timbering to minimize the conductive heat transferred from the ground. The schematic of the apparatus is shown in Figure 2C. Polystyrene foam was used as the heat insulator, with the external surfaces covered by reflecting aluminum mirrors to prevent heating from incident sunlight. The custom-fabricated NCF was fixed atop the thermal emitter with a small air gap, serving as a solar reflector and convection shield.[48]

The temperature difference of the two devices are compared with the thermal images captured in the midday, as shown in Figure 2D. The NCF protected the black emitter from overheating caused by absorption of solar radiation. For instance, temperature of the bare emitter was 45.0 °C under direct sunlight, while that of the NCF-based emitter was only 33.1 °C. Details can be found in Figure S6.

During the 24-hour measurement (see Figure 2E), the real-time relative humidity and wind speed are plotted in Figure 2E-(i), while the stagnation temperature of two emitter surfaces and ambient are plotted in Figure 2E-(ii), along with the coinstantaneous solar irradiance. The solar irradiance fluctuated greatly due to the cloud cover, which slightly deteriorated the radiative cooling effects[8]. The average daytime solar irradiance was ~396 W/m^2. Moreover, the ambient temperature (grey curve) increased with the solar irradiance, which was higher in the daytime with an average of 32.8 °C, and dropped to 27.3 °C at night.

We observed that the temperature of the bare cooling device (black curve) closely followed the solar irradiance with distinct fluctuation during the daytime, which could soar up to 49.8 °C at noon. The temperature of the bare case in the daytime was much higher than that of the ambient, while that in the nighttime was more stable and ~4 °C below the ambient. In contrast, the NCF-based radiative cooler (blue curve) constantly maintained a lower temperature than the ambient during the test, with an average daytime temperature reduction of ~4.9 °C. The NCF, with favorable spectral selectivity, helps to minimize solar absorption and transmit thermal radiation from the emitter, as well as to suppress non-radiative heat transferred. As shown in the inset of Figure 2E-(ii), a remarkable stagnation-temperature reduction of ~17.1 °C was contributed by the

NCF. When the solar irradiance peaked at ~800 W/m^2, the emitter surface reached a temperature of ~3.2 °C below the ambient. Detailed experimental data for the stagnation temperature test are provided in Table S1.

To further explore the cooling capacity of the NCF, we then conducted additional thermal measurements using a feedback-controlled electric heating system[10] (see Figure S7). We eliminated the effect of non-radiative heat transferred between the emitter surface and ambient by keeping them at the same temperature. Under this circumstance, the electric heating power generated by the heater offset the radiative cooling power of the emitter surface because all other heat fluxes were ruled out due to the zero-temperature difference, and thus the net radiative cooling power of the NCF-based radiative cooler was obtained. Detailed results are shown in Figure 2F, with environmental parameters in Figure 2F-(i), temperatures of the emitter surface and ambient in Figure 2F-(ii), surface-ambient temperature differences in Figure 2F-(iii), and net radiative cooling powers along with recorded solar irradiance in Figure 2F-(iv).

It can be seen that the surface temperature tightly tracked ambient temperature with the assistance of the heater. The temperature was stable at ~26 °C in the nighttime but fluctuated greatly in the daytime affected by local wind speed and solar radiation. The frequent fluctuations in the daytime caused the momentary oscillations in the feedback-controlled loop, resulting in greater temperature differences between the surface and ambient. However, the mismatch between the two temperatures is constantly less than 1 °C during the test, as shown in Figure 2F-(iii). We further compared the histogram of the surface-ambient temperature difference during the daytime and nighttime in the inset of Figure 2F-(ii). The temperature difference was more stable in the nighttime and less than ± 0.1 °C, while that in the daytime mainly distributed between 0 and ± 0.5°C.

As shown in Figure 2F-(iv), the NCF-based radiative cooler achieved an average net radiative cooling power of 48 W/m^2 throughout the testing period, with the value being 41 W/m^2 during the daytime (5:30-19:00) and increasing to 55 W/m^2 during the nighttime (19:00-5:30^{+1}). Parasitic solar absorption deteriorated the cooling performance of the emitter. In particular, the net radiative cooling power around noon was only ~20 W/m^2 when exposed to intense solar irradiance of ~800 W/m^2. Detailed experimental data for the net radiative cooling power test are provided in Table S2.

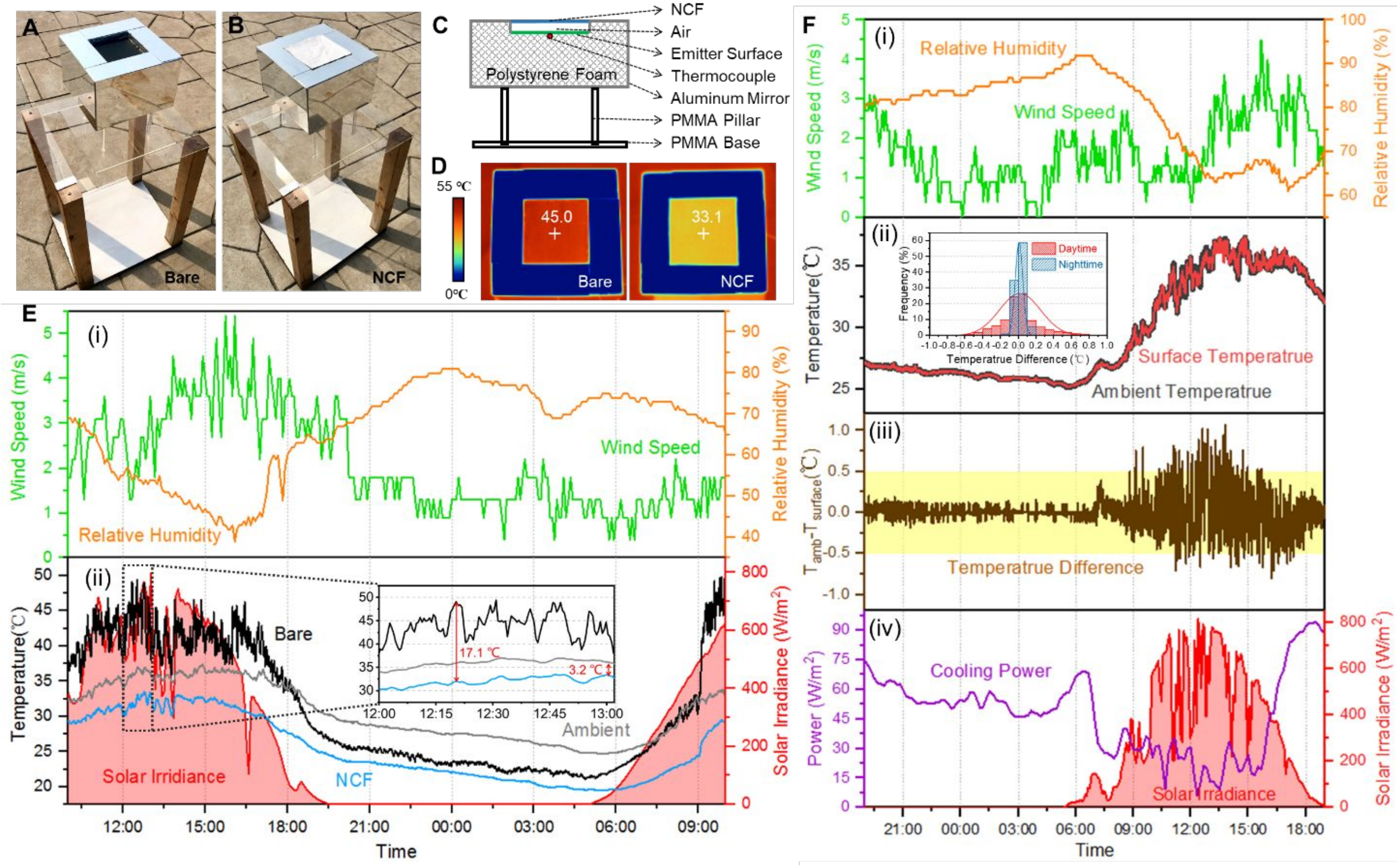

Figure 2. Radiative cooling performance of the NCF-based radiative cooler. Photos of the outdoor experimental devices (A) Bare cooling device and (B) NCF-based radiative cooling device. (C) Schematic of the NCF-based radiative cooler. (D) Thermal images of the bare and NCF-based radiative cooling devices. (E) Temperature

test for the NCF-based radiative cooler. (i) Wind speed and relative humidity during the test, and (ii) Sub-ambient temperature drops with recorded solar irradiance, inset shows the temperature of ambient and the two devices during the midday (12:00-13:00). (F) Thermal measurement for the NCF-based radiative cooler. (i) Wind speed and relative humidity during the test, (ii) Temperatures of the emitter surface and ambient, inset shows the distribution of surface-ambient temperature differences, (iii) Surface-ambient temperature differences, and (iv) Net radiative cooling powers of the NCF-based radiative cooler, along with recorded solar irradiance.

Durability performance Measurements. Apart from the above radiative properties, it is necessary to evaluate the durability performance of the NCF for long-term outdoor applications. Firstly, considering the reliability of outdoor exposure and UV aging, the UHMWPE was selected as the raw material for the NCF, which only has the simplest methylene structure without polar bonds, resulting in superior chemical resistance.[49] It has been demonstrated that the composite fabric hardly absorbs UV,[44] and there is no significant effect on the FTIR spectra for the UHMWPE aged at 80 °C and 120 days.[50] Moreover, we performed several tests on the proposed NCF, including hydrophilicity, mechanical strength, and thermostability.

As shown in Figure 3A, the contact angle slightly decreased along with the reacting time, from the initial contact angle of ~140.7° to ~109° after 20 min, suggesting that the NCF is hydrophobic and has a good waterproofing capacity that can resist potential rain and condensation problems. This is attributed to the aliphatic C−C and C−H bonds of the UHMWPE as well as the nanoporous structure. The contact angle images with different reacting times are supplied in Figure S8.

According to Figure 3B, the NCF can withstand a tensile strength of 23.23 MPa, which is twice as much as that of the PE film. It is satisfactory to withstand extreme weather conditions, such as strong winds and even hail in outdoor environments. Meanwhile, the destroyed strain is ~65%, indicating better toughness with higher elongation compared to the conventional convection shield, i.e., thin PE film.[51] The excellent mechanical performance of the NCF is owing to the composite medium of polyester fabric. Additionally, the porous UHMWPE mostly exists in the warp and weft yarn gaps of the fabric (as shown in Figure 1D), therefore, the tensile or compressive stress will mainly concentrate on the non-deformable fabric rather than on the UHMWPE part. That is, the porous structure of the UHMWPE phase will not deform conspicuously when the composite film is stressed.

The TGA result in Figure 3C shows the decomposition temperature of the NCF is ~400 °C, which is much higher than the operating temperature. The derivative thermogravimetric (DTG) curve peaks at 443.9 °C with a weight loss rate of -39.65 %/min. We only observed one step in the whole thermogravimetric test with a total decomposition of ~84%, illustrating that the decomposition temperature of the UHMWPE and polyester fabric are very close.

In summary, the above results indicate that the NCF has good resistance against rain, hail, strong wind, UV exposure, and thermal aging, proving long-term durability for outdoor applications.

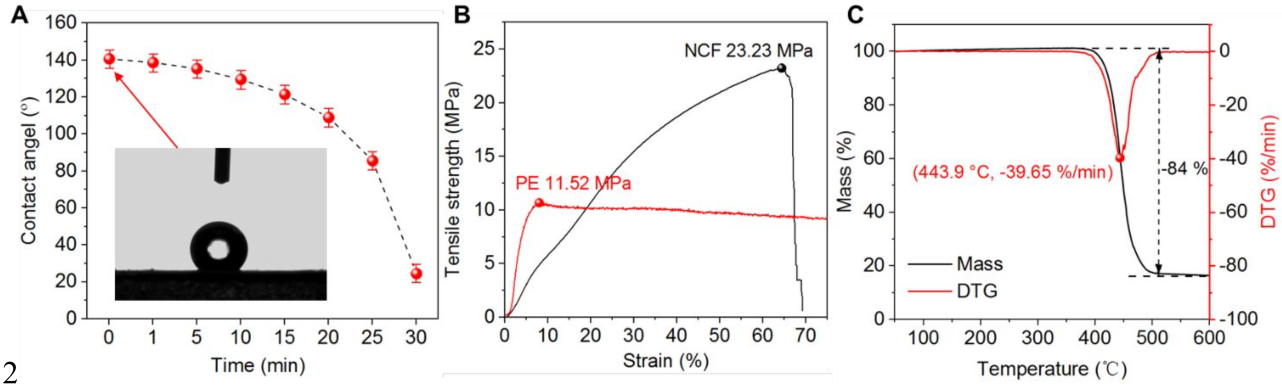

Figure 3. Durability measurements for the NCF. (A) Water contact angles with different reacting times (The error bars correspond to standard deviation caused by the statistical uncertainty in measurement). Inset is the initial water contact angle image at 0 min. (B) Tensile strength test. (C) TGA curves of the NCF.

Modeling Cooling Potential. The NCF is an attractive alternative to other complex, costly, and fragile radiative cooling materials. Despite the above measurements that carried out in a mid-latitude region with high relative humidity and abundant cloud cover, we further modeled the cooling potential of the NCF under various working conditions. To demonstrate the accuracy of the theoretical model presented in Note S3, the modeling results and the above experimental data in Figure 2E are compared in Figure S10.

We selected four representative materials for emitters in the modeling: carbon black (CB),[52] commercial 3M enhanced specular reflector (ESR) film,[53] poly (vinylidene fluoride-co-hexa-fluoropropene) (PVDF-HFP),[54] and multilayer photonic structure (MPS).[4] The emissivity spectral properties of the four materials are shown in Figure 4A-(i). For instance, the CB has near-unit emissivity in the whole wavelengths, performing as a broadband black emitter. However, the rest materials have particularly low emissivity in the solar spectrum, indicating that tiny amounts of solar radiation can be absorbed by the emitters. The weighted average solar reflectivity of the ESR, PVDF-HFP, and MPS is 94.2%,[53] 95%,[54] and 97%,[4] respectively. In the IR spectra, the ESR has broader emissivity, followed by the PVDF-HFP and MPS. Nevertheless, the MPS demonstrates the best selective emissivity in the ATW.

Similar to the above experimental results in Figure 2E-(ii), the bare CB case (black solid line in Figure 4A-(ii)) cannot achieve sub-ambient radiative cooling under direct sunlight. However, a temperature reduction of ~5.7 °C and a net radiative cooling power of ~60 W/m^2 is achieved by the NCF-based case (black dashed line in Figure 4A-(ii)). Moreover, results show that the stagnation temperature of bare ESR and MPS cases is ~3.5 °C below the ambient, and ~5.4 °C for bare PVDF-HFP case. These modeling results are consistent with the practical demonstrations in the previous studies.[4,13,55] When covered by the NCF, the stagnation temperatures of the MPS, ESR, and PVDF-HFP are much lower than those of the bare ones, with the temperature reduction being 7.9 °C, 9.1 °C, and 9.8 °C, respectively. The further temperature reduction is attributed by the NCF with strong solar reflection and non-radiative heat flux suppression. In addition, a considerable cooling power of ~100 W/m^2 can be achieved by the NCF-based PVDF-HFP case, against intense solar irradiance of 850 W/m^2. The employment of the NCF can effectively improve the cooling performance, especially for emitters with undesired solar reflectivity. That means the NCF enables the use of simpler emitters with unfavorable solar reflectivity but good thermal emissivity, relieving the demand for high solar reflection of beneath thermal emitters. Further comparative studies on the cooling performance of the NCF against other potential convection shield materials can be found in Figure S11.

We also predicted the temperature reduction and net radiative cooling power of the NCF-based radiative cooler in different regions of China based on meteorological parameters in the typical year during the cooling season.[56] The average hourly meteorological data during the daytime were obtained from the EnergyPlus,[57] including solar irradiance, ambient temperature, dew point temperature, wind speed, and cloud cover, which are listed in Table S3. The cooling season of different regions can be found in Table S4. Profiles of temperature reduction and net radiative cooling power are highly correlated nationwide (see Figures 4B and 4C). The NCF-based radiative cooler shows greater cooling potential in the Northwest than in the Southeast. More specifically, the temperature reduction increases from -0.4 °C in Shanghai to 4.18 °C in Tibet, while the net radiative cooling power increases from 0.75 W/m^2 to 41.75 W/m^2. Some coastal regions in the Southeast cannot achieve daytime sub-ambient radiative cooling, mainly due to the local humid atmosphere. The results are consistent well with the experimental ones in Hong Kong[58] and Shanghai.[27] The maximum net radiative cooling power occurs in Qinghai, with the value being 43.46 W/m^2, which is attributed by low relative humidity and thin atmosphere in this region.[59] Considering that the average cooling load of energy-efficient residential buildings in most regions of China is less than 10 W/m^2 in the cooling season,[60] passive radiative cooling technology with the NCF can cover the cooling demand in most regions of China.

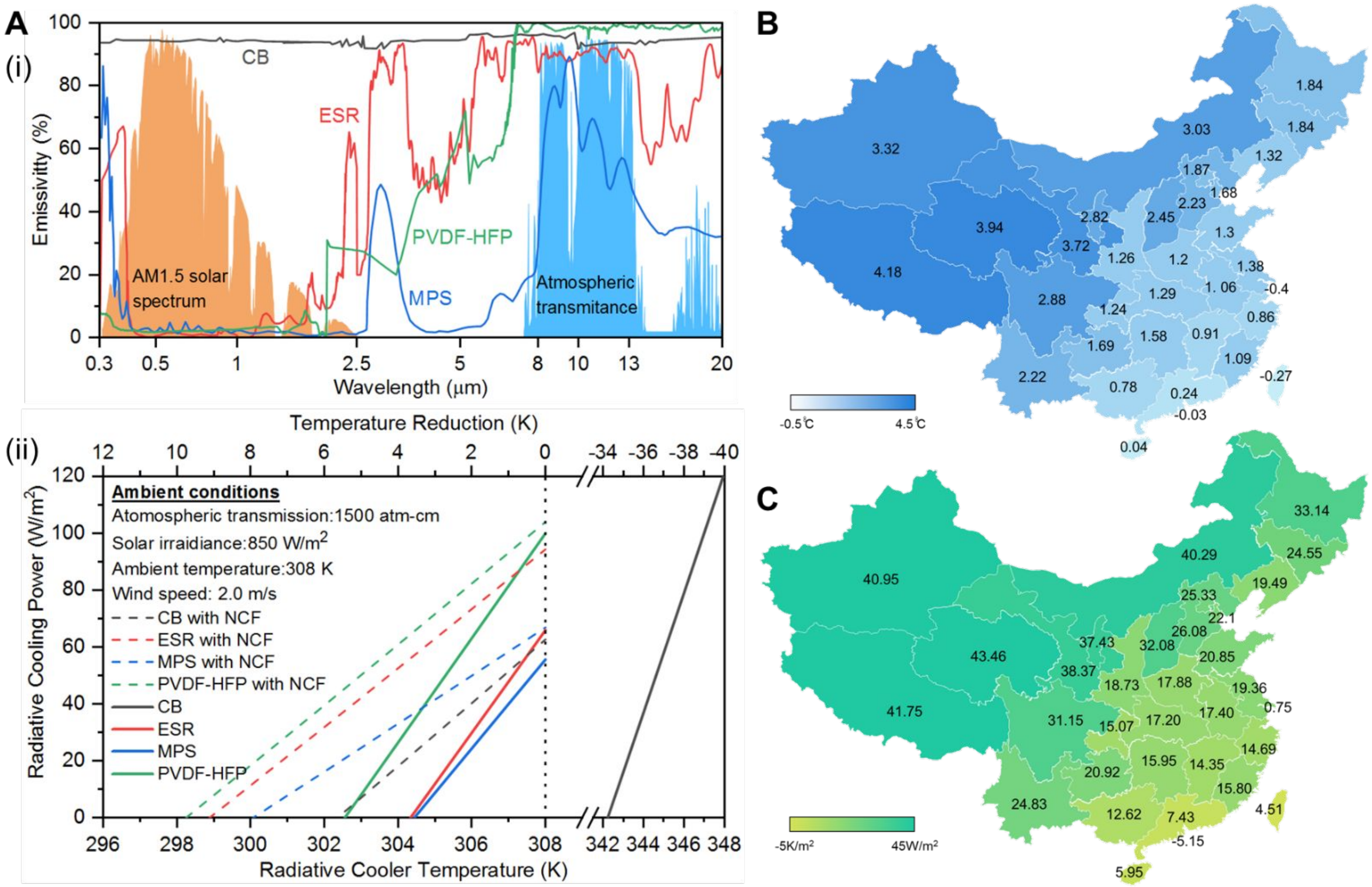

Figure 4. Modeling cooling potential by using the NCF. (A) Cooling potential with different emitters in arid regions. (i) Emissivity spectral profiles of four selected emitters, and (ii) theoretical daytime cooling power potential. Profiles of (B) temperature reduction and (C) net radiative cooling power of the NCF-based radiative cooler in China.

CONCLUSIONS

In summary, we fabricated a convection shield composed of nanoporous composite fabric (NCF) using low-cost materials via a scalable fabrication process. The NCF exhibits near-perfect spectral selectivity with a solar reflectivity of ~95% and an IR transmissivity of ~84%, and favorable UV-resistance, mechanical strength, hydrophilicity, and thermostability. We demonstrated a continuous sub-ambient cooling performance with an average daytime temperature reduction of ~4.9 °C and an average net radiative cooling power of 48 W/m^2 over the 24-hour period. Further modeling results indicated that a temperature reduction of ~10 °C and a net radiative cooling power exceeding 100 W/m^2 can be achieved under direct solar irradiance of 850 W/m^2. Moreover, radiative cooling technology with the NCF can cover cooling demand of energy-efficient residential buildings in most regions of China. This convection shield can be easily applied and removed on various substrates repeatedly, not only improving the cooling performance but also protecting the beneath thermal emitters from harsh weather. More compelling, the NCF enables the use of simpler thermal emitters with unfavorable solar reflectivity but good thermal emissivity, which can pave the way for wider deployment of direct daytime sub-ambient radiative cooling. In addition to acting as the convection shield for radiative cooling modules, the NCF also shows the potential of being personal radiative thermal management textiles.

EXPERIMENTAL SECTION

Materials. The UHMWPE powders with a viscosity average molecular weight of 1.6*10^6 g/mol were provided by Shanghai Research Institute of Chemical Industry Co., Ltd., China. #70 paraffin oil, used as the diluent, was offered by Shanghai Shanyang Lubrication Co., Ltd., China. Irganox 1076 (b-(3,5-bis-tertiary butyl-4-hydroxyphenyl) purity >99.9%), used as the antioxidant, was supplied by Qingdao Usolf Chemical Industry Co., Ltd., China. Dichloromethane was obtained from Shanghai Yunli Economic and Trade Co., Ltd., China. Polyester fabrics (110-μm-thick) with loose warp/weft weaves were commercial products, which were selected as the middle layer of the composite to gain mechanical strength, and the linear density was 90 dtex.

Fabrication. The fabrication could be divided into three main processes as shown in Figure 1E. First, 5 wt% UHMWPE/paraffin oil suspension was melt-mixed in a twin-screw extruder (Thermo Scientific Process 11) at 200 °C with a rotor speed of 60 rpm.

To stabilize the products, 0.7 wt% Irganox 1076 was added into the blends. After that, the homogeneous solution was compressed into a film. Second, one piece of polyester fabric was sandwiched between two pieces of the self-made UHMWPE/paraffin oil film, then those three pieces were put into a self-made mold (250*250*0.5 mm) which was heated in a plate vulcanizing machine (YX-25, Shanghai Xima Rubber & Plastic Equipment Co., Ltd., China) to 190 °C under the pressure of 2 MPa for 20 min to ensure the UHMWPE/paraffin oil solution immersed into the woven fabric and wrap the fabric yarns. Finally, the UHMWPE/paraffin oil/polyester composite fabric was immersed in cold water to initiate the TIPS at room temperature, then the paraffin oil was removed by ultrasonic extraction with dichloromethane for three times. After being dried, the NCF was obtained.

Characterizations. The morphological features of the composite fabric were observed by optical microscopy (BX51-P, OLYMPUS, Japan). The internal microstructure of the NCF was observed by field emission scanning electron microscopy (FE-SEM, S-4800, Hitachi, Japan) at 5.0 kV. The porosity measurement was based on Archimedes' principle, while the density was calculated from its measured volume and mass. The spectral reflectivity between 0.3 and 2.5 μm was measured using an ultraviolet–visible–near-infrared (UV-Vis-NIR) spectrophotometer (Lambda 950, Perkin Elmer) with integrating sphere accessory. The total IR transmissivity was measured using a Fourier transform infrared (FTIR) spectrometer (Spectrum BXII, Perkin Elmer) with a gold-coated integrating sphere accessory. The tensile measurement of the NCF was performed with an Instron 4465 instrument at room temperature with the relative humidity being ~50%, the initial gauge length and width were 50 and 20 mm, respectively, the drawing speed was 40 mm/min. The hydrophilicity of the film was measured using a contact angle goniometer (OCA40Micro, Germany), the droplet volume used for static contact angle measurements was 3 μL. The thermal stability of the film was determined by thermogravimetric analysis (TGA) with a Perkin-Elmer TGA2050 instrument at the heating rate of 20 °C/min from 30 to 600°C in a nitrogen atmosphere.

Measurements. The outdoor experiments were carried out on the rooftop of the 43rd academic building in Tianjin University (Tianjin, China), in July, 2020. Carbon black plate, well thermal-insulated by polystyrene foam enclosure, were used as the thermal emitter. External surfaces of the polystyrene foam were covered by reflecting aluminum mirrors. The custom-fabricated NCF was fixed atop the thermal emitter with a small air gap, serving as a solar reflector and convection shield. Poly(methyl methacrylate) (PMMA) pillars were employed as the base of the devices (see Figure 2C). The two cooling devices were supported by 1000-mm-height wooden timbering to minimize the conductive heat transferred from the ground. (see Figure 2A and 2B). The temperatures of emitters and ambient were measured by K-type thermocouples (± 0.3°C inaccuracy), which had been calibrated prior to use. A data logger (RX 6032C) was employed to record the sample temperatures every 30 s. The thermocouples that measure emitter temperature were attached in the center below the emitter surface (see Figure 2C). The thermocouples that measure ambient temperature were placed in the thermometer screen next to the experimental devices (within a 1-meter distance), where air can freely pass by but sunlight was blocked. Thermal images were taken by a thermal camera (Ti10, FLUCK) in the outdoor environment. The weather data, including ambient temperature, solar irradiance, relative humidity, and wind speed, were collected by a digital high precision weather station (TRM-ZS2) installed at the same height as the experimental devices (see Figure S12). The uncertainties of these parameters are shown in Table S5. The thermocouple-measured ambient temperature was also compared with the weather station-measured ambient temperature to demonstrate the accuracy of measurement (see Figure S13). In addition, the net radiative cooling power was measured by a feedback-controlled electric heating system, see Figure S7 for details.

ASSOCIATED CONTENT

Supporting Information

Figure S1, Refractive index and extinction coefficient of polyethylene; Figure S2, Modeling absorptivity and transmissivity of 100-μm-thick polyethylene; Note S1, Calculated scattering efficiency factor via Mie theory; Figure S3, Scattering efficiency versus wavelength for air pores of specified radius in the NCF; Note S2, Comparative factor of the scattering efficiency in the solar spectrum and the ATW; Figure S4, Weighted average scattering efficiency in solar and the ATW; Figure S5, Radiative cooling power of the NCF-based radiative cooler with different solar reflectivity and IR transmissivity; Figure S6, Thermal images of the bare and the NCF-based device; Table S1, Detailed experimental data for the stagnation temperature test; Figure S7, Schematic of the heating system used to measure the net radiative cooling power; Table S2, Detailed experimental data for the net radiative cooling power test; Figure S8, Water contact angle images with different reacting times; Note S3, Energy balance for emitter surface; Figure S9, Influence of non-radiative heat transfer coefficient on the cooling power; Figure S10, Modeling and experimental surface temperature results of the NCF-based radiative cooler; Figure S11, Cooling capacity of the NCF comparing with other potential convection shield materials; Table S3, Typical annual average daytime meteorological parameters in China; Table S4, Cooling season of different regions in China; Figure S12, Photo of the weather station; Table S5, Measuring range and uncertainty of the measuring instruments; Figure S13, Comparison of ambient temperature measured using a thermocouple with the data from a weather station.

AUTHOR INFORMATION

Corresponding Authors

Mingke Hu – *Department of Architecture and Built Environment, University of Nottingham, University Park, Nottingham NG7 2RD, UK;* orcid.org/0000-0002-3760-7709; Email: Mingke.Hu@nottingham.ac.uk

Junrong Yu – *State Key Laboratory for Modification of Chemical Fibers and Polymer Materials, College of Materials Science and Engineering, Donghua University, Shanghai 201620, China;* orcid.org/0000-0003-3813-8403; Email: yjr@dhu.edu.cn

Authors

Ji Zhang − *Tianjin Key Laboratory of Indoor Air Environmental Quality Control, College of Environmental Science and Engineering, Tianjin University, Tianjin 300350, China;* orcid.org/ 0000-0002-5077-8940; Email: zhangjitju@tju.edu.cn

Zhihua Zhou – *Tianjin Key Laboratory of Indoor Air Environmental Quality Control, College of Environmental Science and Engineering, Tianjin University, Tianjin 300350, China;* orcid.org/0000-0002-7271-1755; Email: zhuazhou@tju.edu.cn

Huajie Tang − *Tianjin Key Laboratory of Indoor Air Environmental Quality Control, College of Environmental Science and Engineering, Tianjin University, Tianjin 300350, China;* Email: tanghuajie@ tju.edu.cn

Jincheng Xing − *Tianjin Key Laboratory of Indoor Air Environmental Quality*

Control, College of Environmental Science and Engineering, Tianjin University, Tianjin 300350, China; Email: xingjincheng@tju.edu.cn

Jiayou Quan − *State Key Laboratory for Modification of Chemical Fibers and Polymer Materials, College of Materials Science and Engineering, Donghua University, Shanghai 201620, China;* orcid.org/0000-0002-9588-2119; Email: qjy@mail.dhu.edu.cn

Junwei Liu − *Tianjin Key Laboratory of Indoor Air Environmental Quality Control, College of Environmental Science and Engineering, Tianjin University, Tianjin 300350, China;* orcid.org/ 0000-0003-4023-6694; Email: jwliu628@tju.edu.cn

Notes

The authors declare no competing financial interest.

ACKNOWLEDGMENTS

This work was supported by Tianjin Municipal Science and Technology Commission (Contract No. 18ZXAQSF00030). The authors are thankful to anonymous reviewers for their valuable comments and feedback.

REFERENCES

(1) Lin, K. Te; Han, J.; Li, K.; Guo, C.; Lin, H.; Jia, B. Radiative Cooling: Fundamental Physics, Atmospheric Influences, Materials and Structural Engineering, Applications and Beyond. *Nano Energy* **2021**, *80*, No. 105517.

(2) Smith, G.; Gentle, A. Energy Savings from the Sky. *Nat. Energy* **2017**, *2*, No. 17142.

(3) Chen, Z.; Zhu, L.; Raman, A.; Fan, S. Radiative Cooling to Deep Sub-Freezing Temperatures through a 24-h Day-Night Cycle. *Nat. Commun.* **2016**, *7*, 1–5.

(4) Raman, A. P.; Anoma, M. A.; Zhu, L.; Rephaeli, E.; Fan, S. Passive Radiative Cooling below Ambient Air Temperature under Direct Sunlight. *Nature* **2014**, *515*, 540–544.

(5) Shi, N. N.; Tsai, C. C.; Camino, F.; Bernard, G. D.; Yu, N.; Wehner, R. Keeping Cool: Enhanced Optical Reflection and Radiative Heat Dissipation in Saharan Silver Ants. *Science* **2015**, *349*, 298–301.

(6) Zhao, D.; Aili, A.; Zhai, Y.; Xu, S.; Tan, G.; Yin, X.; Yang, R. Radiative Sky Cooling: Fundamental Principles, Materials, and Applications. *Appl. Phys. Rev.* **2019**,

6, No. 021306.

(7) Kecebas, M. A.; Menguc, M. P.; Kosar, A.; Sendur, K. Passive Radiative Cooling Design with Broadband Optical Thin-Film Filters. *J. Quant. Spectrosc. Radiat. Transf.* **2017**, *198*, 1339–1351.

(8) Zhao, D.; Aili, A.; Zhai, Y.; Lu, J.; Kidd, D.; Tan, G.; Yin, X.; Yang, R. Subambient Cooling of Water: Toward Real-World Applications of Daytime Radiative Cooling. *Joule* **2019**, *3*, 111–123.

(9) Rephaeli, E.; Raman, A.; Fan, S. Ultrabroadband Photonic Structures To Achieve High-Performance Daytime Radiative Cooling. *Nano Lett*. **2013**, *13*, 1457–1461.

(10) Zhai, Y.; Ma, Y.; David, S. N.; Zhao, D.; Lou, R.; Tan, G.; Yang, R.; Yin, X. Scalable-Manufactured Randomized Glass-Polymer Hybrid Metamaterial for Daytime Radiative Cooling. *Science* **2017**, *355*, 1062–1066.

(11) Ao, X.; Hu, M.; Zhao, B.; Chen, N.; Pei, G.; Zou, C. Preliminary Experimental Study of a Specular and a Diffuse Surface for Daytime Radiative Cooling. *Sol. Energy Mater. Sol. Cells* **2019**, *191*, 290–296.

(12) Atiganyanun, S.; Plumley, J. B.; Han, S. J.; Hsu, K.; Cytrynbaum, J.; Peng, T. L.; Han, S. M.; Han, S. E. Effective Radiative Cooling by Paint-Format Microsphere-Based Photonic Random Media. *ACS Photonics* **2018**, *5*, 1181–1187.

(13) Mandal, J.; Fu, Y.; Overvig, A. C.; Jia, M.; Sun, K.; Shi, N. N.; Zhou, H.; Xiao, X.; Yu, N.; Yang, Y. Hierarchically Porous Polymer Coatings for Highly Efficient Passive Daytime Radiative Cooling. *Science* **2018**, *362*, 315–319.

(14) Heidarinejad, M.; Dalgo, D.; Mi, R.; Zhao, X.; Song, J. A Radiative Cooling Structural Material. *Science*. **2019**, *763*, 760–763.

(15) Liu, J.; Zhang, D.; Jiao, S.; Zhou, Z.; Zhang, Z.; Gao, F. Daytime Radiative Cooling with Clear Epoxy Resin. *Sol. Energy Mater. Sol. Cells* **2020**, *207*, No. 110368.

(16) Berdahl, P.; Akbari, H.; Levinson, R.; Miller, W. A. Weathering of Roofing Materials - An Overview. *Constr. Build. Mater*. **2008**, *22*, 423–433.

(17) Sun, K.; Riedel, C. A.; Wang, Y.; Urbani, A.; Simeoni, M.; Mengali, S.; Zalkovskij, M.; Bilenberg, B.; De Groot, C. H.; Muskens, O. L. Metasurface Optical Solar Reflectors Using AZO Transparent Conducting Oxides for Radiative Cooling of Spacecraft. *ACS Photonics* **2018**, *5*, 495–501.

(18) Hu, M.; Suhendri; Zhao, B.; Ao, X.; Cao, J.; Wang, Q.; Riffat, S.; Su, Y.; Pei, G. Effect of the Spectrally Selective Features of the Cover and Emitter Combination on Radiative Cooling Performance. *Energy Built Environ*. **2020**, in process.

(19) Peng, Y.; Chen, J.; Song, A. Y.; Catrysse, P. B.; Hsu, P.-C.; Cai, L.; Liu, B.; Zhu, Y.; Zhou, G.; Wu, D. S.; Lee, H. R.; Fan, S.; Cui, Y. Nanoporous Polyethylene Microfibres for Large-Scale Radiative Cooling Fabric. *Nat. Sustainability* **2018**, *1*, 105−112.

(20) Xiao, R.; Hou, C.; Yang, W.; Su, Y.; Li, Y.; Zhang, Q.; Gao, P.; Wang, H. Infrared-Radiation-Enhanced Nanofiber Mirembrane for Sky Radiative Cooling of the Human Body. *ACS Appl. Mater. Interfaces* **2019**, *11*, 44673–44681.

(21) Song, Y.; Lei, M.; Deng, L.; Lei, J.; Li, Z. Hybrid Metamaterial Textiles for Passive Personal Cooling Indoors and Outdoors. *ACS Appl. Polym. Mater.* **2020**, *2*, 4379-4386.

(22) Yang, M.; Yang, M.; Zou, W.; Zou, W.; Guo, J.; Guo, J.; Qian, Z.; Qian, Z.; Luo, H.; Luo, H.; Yang, S.; Yang, S.; Zhao, N.; Zhao, N.; Pattelli, L.; Pattelli, L.; Xu, J.; Wiersma, D. S.; Wiersma, D. S. Bioinspired "Skin" with Cooperative Thermo-Optical Effect for Daytime Radiative Cooling. *ACS Appl. Mater. Interfaces* **2020**, *12*, 25286–25293.

(23) Kim, H.; McSherry, S.; Brown, B.; Lenert, A. Selectively Enhancing Solar Scattering for Direct Radiative Cooling through Control of Polymer Nanofiber Morphology. *ACS Appl. Mater. Interfaces* **2020**, *12*, 43553–43559.

(24) Torgerson, E.; Hellhake, J. Polymer Solar Filter for Enabling Direct Daytime Radiative Cooling. *Sol. Energy Mater. Sol. Cells* **2019**, *206*, No. 110319.

(25) Leroy, A.; Bhatia, B.; Kelsall, C. C.; Castillejo-Cuberos, A.; Di Capua, M. H.; Zhao, L.; Zhang, L.; Guzman, A. M.; Wang, E. N. High-Performance Subambient Radiative Cooling Enabled by Optically Selective and Thermally Insulating Polyethylene Aerogel. *Sci. Adv.* **2019**, *5*, 1–9.

(26) Zhu, L.; Raman, A.; Fan, S.; Zhu, L.; Raman, A.; Fan, S. Color-Preserving Daytime Radiative Cooling Color-Preserving Daytime Radiative Cooling. *Appl. pgysics Lett*. **2013**, *103*, No. 223902.

(27) Bao, H.; Yan, C.; Wang, B.; Fang, X.; Zhao, C. Y.; Ruan, X. Double-Layer Nanoparticle-Based Coatings for Efficient Terrestrial Radiative Cooling. *Sol. Energy Mater. Sol. Cells* **2017**, *168*, 78–84.

(28) Johnson, T. E. Radiation Cooling of Structures with Infrared Transparent Wind Screens. *Sol. Energy* **1975**, *17*, 173–178.

(29) Bosi, S. G.; Bathgate, S. N.; Mills, D. R. At Last ! A Durable Convection Cover for Atmospheric Window Radiative Cooling Applications. *Energy Procedia* **2014**, *57*,

1997–2004.

(30) Benlattar, M.; Oualim, E. M.; Mouhib, T.; Harmouchi, M.; Mouhsen, A.; Belafhal, A. Thin Cadmium Sulphide Film for Radiative Cooling Application. *Opt. Commun.* **2006**, *267*, 65–68.

(31) Zhao, B.; Ao, X.; Chen, N.; Xuan, Q.; Hu, M.; Pei, G. General Strategy of Passive Sub-Ambient Daytime Radiative Cooling. *Sol. Energy Mater. Sol. Cells* **2019**, *199*, 108–113.

(32) Hu, M.; Zhao, B.; Ao, X.; Feng, J.; Cao, J.; Su, Y.; Pei, G. Experimental Study on a Hybrid Photo-Thermal and Radiative Cooling Collector Using Black Acrylic Paint as the Panel Coating. *Renew. Energy* **2019**, *139*, 1217–1226.

(33) Hjortsberg, A.; Granqvist, C. G. Radiative Cooling with Selectively Emitting Ethylene Gas. *Appl. Phys. Lett*. **1981**, *39*, 507–509.

(34) Nilsson, N. A.; Eriksson, T. S.; Granqvist, C. G. Infrared-Transparent Convection Shields for Radiative Cooling: Initial Results on Corrugated Polyethylene Foils. *Sol. Energy Mater*. **1985**, *12*, 327–333.

(35) Gentle, A. R.; Dybdal, K. L.; Smith, G. B. Polymeric Mesh for Durable Infra-Red Transparent Convection Shields: Applications in Cool Roofs and Sky Cooling. *Sol. Energy Mater. Sol. Cells* **2013**, *115*, 79–85.

(36) Gulmine, J. V.; Janissek, P. R.; Heise, H. M.; Akcelrud, L. Polyethylene Characterization by FTIR. *Polym. Test*. **2002**, *21*, 557–563.

(37) Palik, E. Handbook of Optical Constants of Solids, *3 Academic Press*, **1998**

(38) Pettersson, L.A.A.; Roman, L.S.; Inganas, O. Modeling photocurrent action spectra of photovoltaic devices based on organic thin films, *J. Appl. Phys.* **1999**, *86*, 487–496.

(39) Xu, Z.; Li, N.; Liu, D.; Huang, X.; Wang, J.; Wu, W.; Zhang, H.; Liu, H.; Zhang, Z.; Zhong, M. A New Crystal $Mg_{11}(HPO_3)_8(OH)_6$ for Daytime Radiative Cooling. *Sol. Energy Mater. Sol. Cells* **2018**, *185*, 536–541.

(40) Tong, J. K.; Huang, X.; Boriskina, S. V.; Loomis, J.; Xu, Y.; Chen, G. Infrared-Transparent Visible-Opaque Fabrics for Wearable Personal Thermal Management. *ACS Photonics* **2015**, *2*, 769–778.

(41) Liu, R.; Wang, X.; Yu, J.; Wang, Y.; Zhu, J.; Hu, Z. Development and Evaluation of UHMWPE/Woven Fabric Composite Microfiltration Membranes via Thermally Induced Phase Separation. *RSC Adv*. **2016**, *6*, 90701–90710.

(42) Xu, X.; Vignarooban, K.; Xu, B.; Hsu, K.; Kannan, A. M. Prospects and Problems

of Concentrating Solar Power Technologies for Power Generation in the Desert Regions. *Renew. Sustain. Energy Rev*. **2016**, *53*, 1106–1131.

(43) Peng, Y.; Cui, Y. Advanced Textiles for Personal Thermal Management and Energy. *Joule* **2020**, *4*, 724–742.

(44) Liu, R.; Wang, X.; Yu, J.; Wang, Y.; Zhu, J.; Hu, Z. A Novel Approach to Design Nanoporous Polyethylene/Polyester Composite Fabric via TIPS for Human Body Cooling. *Macromol. Mater. Eng*. **2018**, *303*, 1–10.

(45) Jafar-Zanjani, S.; Salary, M. M.; Mosallaei, H. Metafabrics for Thermoregulation and Energy-Harvesting Applications. *ACS Photonics* **2017**, *4*, 915–927.

(46) Hsu, P.; Song, A. Y.; Catrysse, P. B.; Liu, C.; Peng, Y.; Xie, J.; Fan, S.; Cui, Y. Radiative Human Body Cooling by Nanoporous Polyethylene Textile. *Science.* **2016**, *353*, 1019–1024.

(47) Reference Solar Spectral Irradiance: Air Mass 1.5 http://rredc.nrel.gov/solar/spectra/am1.5/.

(48) Liu, J.; Zhang, J.; Zhang, D.; Jiao, S.; Xing, J.; Tang, H.; Zhang, Y.; Li, S.; Zhou, Z.; Zuo, J. Sub-Ambient Radiative Cooling with Wind Cover. *Renew. Sustain. Energy Rev*. **2020**, *130*, No. 109935.

(49) Fang, X.; Wyatt, T.; Hong, Y.; Yao, D. Gel Spinning of UHMWPE Fibres with Polybutene as a New Spin Solvent. *Polym. Eng. Sci.* **2016**, *56*, 697–706.

(50) Belotti, L. P.; Vadivel, H. S.; Emami, N. Tribological Performance of Hygrothermally Aged UHMWPE Hybrid Composites. *Tribol. Int.* **2019**, *138*, 150–156.

(51) Pieters, J. G.; Deltour, J. M. R. Performances of Greenhouses with the Presence of Condensation on Cladding Materials. *J. Agric. Eng. Res.* **1997**, *68*, 125–137.

(52) Yalçın, R. A.; Blandre, E.; Joulain, K.; Drévillon, J. Daytime Radiative Cooling with Silica Fiber Network. *Sol. Energy Mater. Sol. Cells* **2020**, *206*. No. 110320.

(53) Gentle, A. R.; Smith, G. B. A Subambient Open Roof Surface under the Mid-Summer Sun. *Adv. Sci*. **2015**, *2*, No. 1500119.

(54) Liu, J.; Zhou, Z.; Zhang, D.; Jiao, S.; Zhang, J.; Gao, F.; Ling, J. Research on the Performance of Radiative Cooling and Solar Heating Coupling Module to Direct Control Indoor Temperature. *Energy Convers. Manag.* **2020**, *205*, No. 112395.

(55) Goldstein, E. A.; Raman, A. P.; Fan, S. Sub-Ambient Non-Evaporative Fluid Cooling with the Sky. *Nat. Energy* **2017**, *2*, 1–7.

(56) Liu, J.; Zhou, Z.; Zhang, D.; Jiao, S.; Zhang, Y.; Luo, L. Field Investigation and Performance Evaluation of Sub-Ambient Radiative Cooling in Low Latitude Seaside.

Renew. Energy **2020**, *155*, 90–99.

(57) Weather data. 2020. https://energyplus.net/weather.

(58) Tso, C. Y.; Chan, K. C.; Chao, C. Y. H. A Field Investigation of Passive Radiative Cooling under Hong Kong's Climate. *Renew. Energy* **2017**, *106*, 52–61.

(59) Zeyghami, M.; Goswami, D. Y.; Stefanakos, E. A Review of Clear Sky Radiative Cooling Developments and Applications in Renewable Power Systems and Passive Building Cooling. *Sol. Energy Mater. Sol. Cells* **2018**, *178*, 115–128.

(60) Liu, J.; Zhang, D.; Jiao, S.; Zhou, Z.; Zhang, Z.; Gao, F. Preliminary Study of Radiative Cooling in Cooling Season of the Humid Coastal Area. *Sol. Energy Mater. Sol. Cells* **2020**, *208*, No. 110412.